Journal of Applied Electrochemistry **31**: 749–757, 2001.

Abnormal infrared effects and electrocatalytic properties of nanometer scale thin film of PtRu alloys for CO adsorption and oxidation†

M-S. ZHENG, S-G. SUN* and S-P. CHEN
Laboratory for Physical Chemistry of Solid Surfaces, Department of Chemistry, Xiamen University, Xiamen 361005, China
*(*author for correspondence, fax: +86 592 2183047, e-mail: sgsun@xmu.edu.cn)*

Received 14 January 2000; accepted in revised form 18 September 2000

Key words: abnormal infrared effects, CO adsorption, nanometer scale thin film, PtRu alloy

Abstract

Nanometer scale thin films of PtRu alloy supported on glassy carbon (nm-PtRu/GC) were prepared using electrochemical codeposition under cyclic voltammetric conditions. The composition of the PtRu alloy was altered by varying the concentration of Pt^{4+} and Ru^{3+} ions in the deposition solution. STM results demonstrated that the nm-PtRu film was composed of crystallites appearing in a layered hexagonal form. The nm-PtRu/GC exhibited a high catalytic activity for CO oxidation, consisting mainly in a negative shift of potential for CO_{ad} oxidation. *In situ* FTIR spectroscopic studies revealed that the nm-PtRu/GC alloy electrodes of different surface composition exhibit abnormal infrared effects (AIREs) as observed on electrodes of nanometer scale thin films of transition metals. The AIREs observed on nm-PtRu/GC electrodes consist in the inversion of CO_{ad} bands, the significant enhancement of IR absorption and an increase in the FWHM. Following the increase in Ru component in the nm-PtRu thin film the FWHM was increased progressively from 20 cm^{-1} on a nm-Pt/GC to 55 cm^{-1} on a nm-Ru/GC electrode, and the enhancement factor of IR absorption by CO_L was between 10.5 to 13.1. The present study has provided new understanding of the structure and properties of nanometer scale thin film PtRu alloy material, and highlights its potential for fuel cell applications.

1. Introduction

The PtRu alloy has been recognized as the best anode catalyst for polymer electrolyte membrane fuel cells (PEMFC), since it exhibits good properties for CO tolerance [1]. Extensive studies on PtRu alloy have been carried out recently [2], and particular interest has focused on the application of these materials as anodes in methanol fuel cells (MFC) for electric vehicles [3]. Different binary Pt–Ru materials have been prepared and tested, such as Ru adatom or Ru nanoparticles modified Pt polycrystal [4, 5] and Pt single crystal electrodes [6–9], PtRu nanoparticles [10–12], PtRu bulk alloys [13–20], and carbon supported PtRu alloys derived from electrochemical codeposition [21–25]. The studies demonstrated that the alloy PtRu material with a composition of Pt:Ru = 1:1 exhibits the highest activity for CO oxidation [20–22]. As the properties of PtRu electrocatalysts depend on the alloy composition, the crystallite size and the surface structure, it may be convenient to prepare PtRu alloy using electrochemical codeposition, in which the above parameters can be easily manipulated. Although *in situ* infrared spectroscopy has been applied widely in studies of electrocatalysis relating to fuel cells, especially in the electrocatalytic oxidation of small organic molecules [26], very few papers have been published concerning *in situ* IR studies of CO and CH_3OH adsorption and oxidation on PtRu alloy electrodes [13, 15–17, 19, 24]. *In situ* infrared spectroscopy can provide information on electrochemical reactions at a molecule level, which can contribute to the details of reaction mechanisms [26]. Moreover, together with a test molecular reaction such as CO adsorption *in situ* IR spectroscopy can also be used to study electrode surface processes [27]. We have recently shown that a nanometer scale thin film of transition metals electrodeposited on glassy carbon and other supports exhibited abnormal infrared effects (AIREs) [24, 28–30], that is, the CO or other molecules adsorbed on the thin film give rise to three abnormal IR features in comparison with the IR features of the same molecule adsorbed on the corresponding massive metal electrode: (i) inversion of the direction of the IR band, (ii) significant enhancement of the intensity of the IR band and (iii) increase in the full width at half maximum (FWHM) of the IR band. The AIREs were ascribed to a

† Paper presented at the workshop on "Electrocatalysis in direct and indirect methanol fuel cells" held at Portoroz, Slovenia, September 1999.

kind of nanosize effect of material and have initiated follow up studies [31, 32].

To study the electrocatalytic properties of nanometer thin PtRu alloy films and also to study further the AIREs, the adsorption and oxidation of CO were used as test molecule reactions in the present study, and new results were obtained by using cyclic voltammetry, scanning tunneling microscopy and *in situ* FTIR spectroscopy.

2. Experimental details

The nanometer-thin films of Pt, Ru and PtRu alloy supported on glassy carbon were prepared by electrodeposition under cyclic voltammetric conditions. The substrate of glassy carbon (GC) of 6 mm in diameter was sealed into a Teflon support and polished mechanically using sandpaper and alumina powder of size 5, 1, 0.3 down to 0.05 μm to obtain a mirror finish before PtRu deposition. The composition and film thickness of the PtRu alloy were controlled by varying the concentration of Pt^{4+} and Ru^{3+} ions in the solution and altering the potential cycling of deposition. In general, PtRu alloy films of a few tens of nanometers in thickness were prepared and the film electrode was denoted as nm-PtRu/GC. In the cyclic voltammetry for PtRu deposition the upper and lower cycling limits were fixed at 0.4 V and -0.5 V, and the sweep rate was 50 mV s^{-1}. A saturated calomel electrode (SCE) was used as reference electrode and an EG & G potentiostat/galvanostat (model 263A) was used in electrochemical measurements.

Before the adsorption of CO, the nm-PtRu/GC electrode was subjected to potential cycling in 0.1 M H_2SO_4 between -0.25 to 0.5 V until a stable cyclic voltammogram was achieved. The saturation CO adlayer was obtained by bubbling CO into 0.1 M H_2SO_4 solution and potential cycling between -0.25 and 0.0 V until the hydrogen adsorption current had been completely suppressed. To investigate solely adsorbed CO (CO_{ad}), the dissolved CO species were removed by bubbling N_2 into the solution while holding the electrode potential at 0.0 V. In such a way only adsorbed CO was subjected to investigation.

In situ FTIR spectra were acquired on a Nicolet 730 FTIR spectrometer equipped with a Gopher infrared source and liquid nitrogen cooled MCT-B detector. The spectral resolution of 8 cm^{-1} was maintained in all IR measurements. A CaF_2 disc IR window and an incident angle of 60° were used in the *in situ* IR set-up (IR cell and reflection accessories). The MS-FTIR procedure [27, 28] was employed in the IR measurements. The resulting spectrum was reported as the relative change in reflectivity calculated as

$$\frac{\Delta R}{R} = \frac{R(E_S) - R(E_R)}{R(E_R)} \quad (1)$$

where $R(E_S)$ and $R(E_R)$ are single-beam spectra of reflection collected at sample potential E_S and reference potential E_R, respectively. 400 interferograms were collected and coadded into each single-beam spectrum in this study. E_S was set at the potential where CO_{ad} species are stable on the electrode surface and E_R was fixed at 0.50 V (for nm-Ru/GC and nm-PtRu/GC) or at 0.70 V (for Pt and nm-Pt/GC), at which the adsorbed CO can be oxidized immediately to CO_2. As a consequence, the adsorbed CO species exist only at E_S. According to Equation 1 a positive going CO_2 band and negative-going CO_{ad} bands will appear in the resulting spectra for normal IR absorption.

A P4-18-SPM scanning probe microscope (NT-MDT Russia) was employed for *ex situ* structural analysis of PtRu thin films in atmosphere and at room temperature.

All solutions were prepared from super pure H_2SO_4, Millipore water supplied from a Milli-Q Lab equipment (Nihon Millipore), and other chemicals of analytical grade. The solutions were deaerated by bubbling N_2 before measurement. All experiments were carried out at room temperature.

3. Results and discussion

3.1. *Studies of cyclic voltammetry*

Figure 1 shows a comparison of the cyclic voltammograms (CVs) recorded on nm-Pt/GC, nm-PtRu/GC and nm-Ru/GC electrodes. The CV features of nm-Pt/GC and nm-Ru/GC (Figure 1(a)) are similar to those observed on supported Pt [30, 33] and Ru [34, 35]. Two current peaks of hydrogen adsorption at around -0.02 and -0.2 V were observed in the CV of nm-Pt/GC. The CV of the nm-Ru/GC electrode shows one current peak of hydrogen adsorption near -0.2 V and a broad current peak of OH adsorption lying between -0.1 and 0.35 V. The current in the double layer region ($0.05 \sim 0.5$ V) is relatively large in the CVs of both electrodes, signifying the influence of the GC substrate. The CVs in Figure 1(b) were recorded on nm-PtRu/GC electrodes prepared from electrodeposition solutions that contain different concentrations of Pt^{4+} and Ru^{3+} ions. The CV features of a nm-PtRu/GC electrode may be regarded as a mixture of those of nm-Pt/GC and nm-Ru/GC electrodes, and vary with the composition of the PtRu alloy prepared. Following the increase in Ru^{3+} concentration in the electrodeposition solution, the hydrogen adsorption–desorption current on surface Pt sites in the potential region between -0.25 and 0.05 V is decreased, while the current of OH adsorption–desorption on surface Ru sites between -0.1 and 0.5 V is augmented. We have shown that the composition of PtRu alloy supported on glassy carbon depends on the ratio of Pt^{4+} and Ru^{3+} concentration in the electrodeposition solution under fixed deposition conditions (i.e., five cycles of potential cycling between -0.5 and 0.4 V at sweep rate

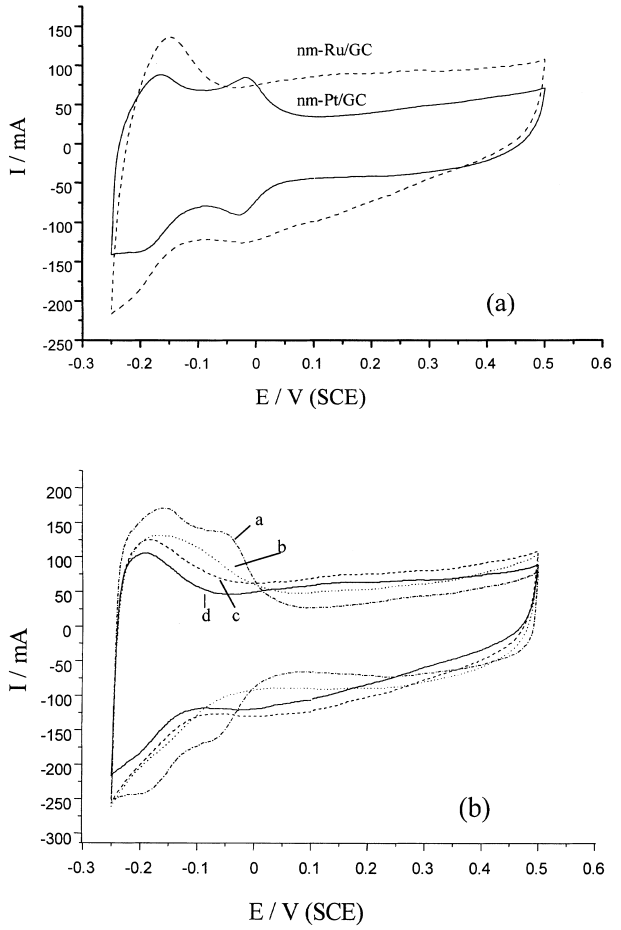

Fig. 1. Cyclic voltammograms of nm-Pt/GC and nm-Ru/GC (a), and nm-PtRu/GC (b) of different compositions: (a) 4:2, (b) 4:4, (c) 4:8, (d) 4:12. 0.1 M $HClO_4$ solution, sweep rate 50 mV s^{-1}.

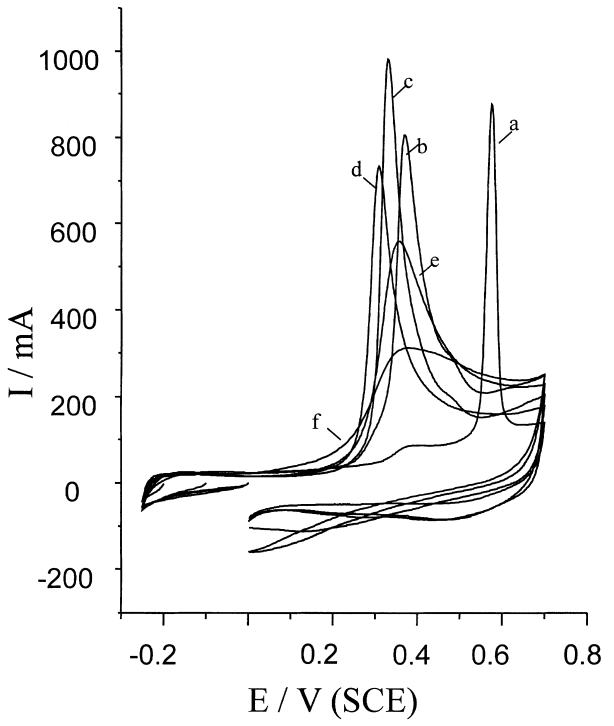

Fig. 2. j/E curves for CO_{ad} oxidation on different nanometer thin film electrodes: (a) nm-Pt/GC, (b) nm-PtRu/GC(4:1), (c) nm-PtRu/GC(4:2), (d) nm-PtRu/GC(4:6), (e) nm-PtRu/GC(4:10) and (f) nm-Ru/GC. 0.1 M $HClO_4$ solution, sweep rate 50 mV s^{-1}.

50 mV s^{-1}). Richarz et al. [21] also demonstrated that the composition of PtRu alloy prepared by electrochemical codeposition depends linearly on the concentration of Pt^{4+} and Ru^{3+} ions in solution. As it is not convenient to measure accurately the content of Pt and Ru in a PtRu alloy film, we denote hereafter the composition of nm-PtRu/GC electrodes by specifying the concentration of Pt^{4+} and Ru^{3+} ions in the electrodeposition solution. Thus a nm-PtRu/GC(4:1) indicates that the electrode was prepared from electrodeposition solution containing 4 mM H_2PtCl_6 and 1 mM $RuCl_3$ in 0.1 M H_2SO_4.

The oxidation of adsorbed carbon monoxide may be employed as a probe reaction to assess the activity of nm-PtRu/GC electrodes. The cyclic voltammograms of oxidation of CO adsorbed on nm-Pt/GC, nm-Ru/GC and on nm-PtRu/GC of different composition are displayed in Figure 2. Significant catalytic characteristics are evident on nm-PtRu/GC and nm-Ru/GC electrodes. The most evident catalytic effect is the negative shift of the potential of the oxidation current peak. The peak position measured from the voltammogram recorded on a nm-Pt/GC electrode is 0.575 V. However, it is shifted negatively to the potential region between 0.3 and 0.4 V in the voltammograms of nm-Ru/GC and nm-PtRu/GC electrodes. The main parameters that characterize the catalytic properties of nanometer thin film electrodes towards CO_{ad} oxidation may be the potential (E_p), the current density (j_p) and the full width at half maximum (FWHM) of the current peak. Under the present conditions saturation coverage of CO adsorption was achieved on each electrode. As a consequence the quantity of electric charge of CO_{ad} oxidation (Q_{CO}^{OX}) can be used as a measure of the surface roughness of the electrode, since the geometric area of the GC substrate has a defined value of 0.28 cm^{-2}. The relative roughness of Ru and PtRu alloy film electrodes with regard to the nm-Pt/GC electrode may be defined as $(Q_{CO}^{OX})/(Q_{CO}^{OX})_{nm\text{-}Pt/GC}$, and the j_p/Q_{CO}^{OX} represents the normalized rate of CO_{ad} oxidation. Table 1 lists parameters measured on different nanometer thin film electrodes. Following the increase in Ru in nm-PtRu/GC alloy electrode the FWHM increased progressively from 27 mV on nm-Pt/GC to 212 mV on nm-Ru/GC, the j_p/Q_{CO}^{OX} decreased from 1.35 s^{-1} on nm-Pt/GC to 0.24 s^{-1} on nm-Ru/GC. It is important to note that the variation of E_p showed a minimum at 308 mV on a nm-PtRu/GC(4:6) electrode. Gasteiger et al. [20] reported that the minimum E_p of CO_{ad} oxidation was measured on a 50:50 PtRu alloy electrode. The present results confirmed that the composition of nm-PtRu/GC(4:6) electrode may be close to a 50:50 PtRu alloy, since it was prepared in a solution containing 4 mM Pt^{4+} and 6 mM Ru^{3+} that is

Table 1. Cyclic voltammogram parameters recorded on different thin film electrodes

Electrode	E_p /mV	FWHM /mV	j_p /μA cm^{-2}	Q_{CO}^{OX} /μC cm^{-2}	(j_p/Q_{CO}^{OX}) /s^{-1}	$Q_{CO}^{OX}/(Q_{CO}^{OX})_{nm\text{-}Pt/GC}$
nm-Pt/GC	575	27	874.9	646.7	1.35	1.0
nm-PtRu/GC(4:1)	370	67	804.1	1666	0.48	2.57
nm-PtRu/GC(4:2)	331	56	978.4	1555	0.63	2.40
nm-PtRu/GC(4:4)	335	53	796.5	1223	0.65	1.89
nm-PtRu/GC(4:6)	308	63	732.1	1364	0.54	2.11
nm-PtRu/GC(4:8)	356	88	562.0	1184	0.48	1.83
nm-PtRu/GC(4:10)	355	128	557.1	1626	0.34	2.51
nm-PtRu/GC(4:12)	357	160	340.1	1163	0.29	1.80
nm-Ru/GC	378	212	289.2	1190	0.24	1.84

near the solution composition of electrodeposition to produce 50:50 PtRu alloy [21, 22]. The relative roughness of nm-Ru/GC and nm-PtRu/GC electrodes is always larger than 1, signifying that the surface of these electrodes is rougher than the nm-Pt/GC electrode under the preparation conditions.

3.2. In situ *FTIR spectroscopy*

In Figure 3 the spectra recorded on nm-Pt/GC, nm-PtRu/GC(4:6) and nm-Ru/GC for E_S at 0.0 V and E_R at 0.5 (nm-PtRu/GC(4:6), nm-Ru/GC) or 0.7 V (nm-Pt/GC) are compared. To discuss the abnormal infrared effects of electrodes of nanometer thin film materials, a spectrum acquired on a massive Pt electrode under the same conditions but multiplied by a factor of 3 is also displayed. We observe from all four spectra a positive-going band near 2343 cm^{-1}, which is assigned to IR absorption of CO_2 species at E_R in the solution of electrode/IR window thin layer. It is evident that the CO_2 species has been derived uniquely from the oxidation of adsorbed CO (CO_{ad}) under the present conditions, and the integrated intensity of the CO_2 band (A_{CO_2}) may be in direct proportion to the quantity of CO_{ad} species. The IR absorption of CO adsorbed on the three nanometer thin film electrodes yields positive-going bands in the region between 2100 and 1750 cm^{-1}, while a negative-going band appears as expected near 2084 cm^{-1} in the case of CO adsorbed on a massive Pt electrode. Moreover, the integrated intensity of the CO_{ad} bands ($A_{CO_{ad}}$) in the spectra recorded on nanometer thin film electrodes is much larger than that measured from the spectrum for CO adsorbed on a massive Pt electrode, that is, the IR absorption of CO adsorbed on electrodes of nanometer thin film materials has been significantly enhanced.

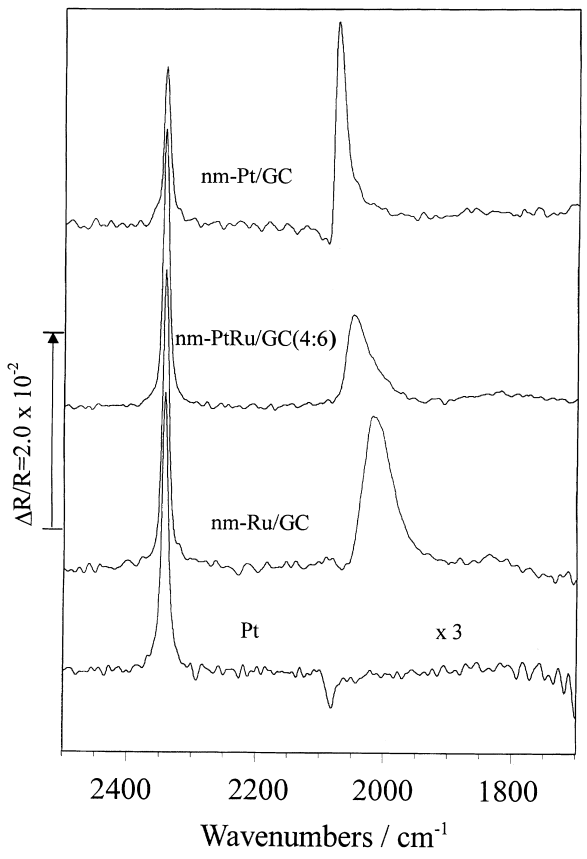

Fig. 3. In situ FTIR spectra of CO adsorbed on different electrodes: (a) nm-Pt/GC, (b) nm-PtRu/GC(4:6), (c) nm-Ru/GC and (d) massive Pt. 0.1 M $HClO_4$ solution, $E_S = 0.0$ V, $E_R = 0.7$ V.

In the spectrum of the nm-Pt/GC electrode, the positive-going band near 2074 cm^{-1} is attributed to IR absorption of linearly adsorbed CO (CO_L). The FWHM of this band is 20 cm^{-1}, which is slightly larger than the FWHM (14 cm^{-1}) measured from the spectrum of massive Pt. Since adsorbed CO existed only at E_S and the CO_2 was derived solely from the oxidation of CO_L at E_R and there is no enhancement of IR absorption by solution CO_2 species, the intensity of the CO_2 band can be used as a measure of the quantity of CO_{ad}. As a consequence, the ratio of the integrated intensity of the CO_{ad} band ($A_{CO_{ad}}$) over that of the CO_2 band (A_{CO_2}); that is, $A_{CO_{ad}}/A_{CO_2}$, can be defined as the normalized intensity of IR absorption of CO_{ad}. A value of 0.13 was measured from the spectrum of massive Pt, and a value of 3.62 was obtained on nm-Pt/GC. The enhancement factor (Δ) of IR absorption, which represents the enhancement of IR absorption of CO adsorbed at a nm-Pt/GC electrode against the same quantity of CO adsorbed on massive Pt, may be calculated using Equation 2 [28–30]:

$$\Delta = \frac{(A_{CO_{ad}}/A_{CO_2})_{nm\text{-}Pt/GC}}{(A_{CO_{ad}}/A_{CO_2})_{Pt}} \quad (2)$$

The enhancement factor of a nm-Pt/GC electrode has been evaluated at 27.8 from data measured in Figure 3.

Two positive-going bands, a large one near 2017 cm^{-1} and a small one around 1830 cm^{-1} appeared in the spectrum of a nm-Ru/GC electrode. It is obvious that the large band near 2017 cm^{-1} is due to IR absorption of CO_L species, and that the small band around 1830 cm^{-1} may be assigned mainly to bridge bonded CO (CO_B) species. However, in considering the wide spread of the small band multibonded CO (CO_m) may also exist. It is interesting to observe that the CO_{ad} bands are all in the same positive-going direction of the CO_2 band, and a typical character of the CO_L band consisting in its large FWHM measured at 55 cm^{-1}. In comparison with the value of 38 cm^{-1} measured on a massive Ru electrode [16], the FWHM of CO_L band on a nm-Ru/GC electrode is significantly increased. If we take the $(A_{CO}/A_{CO_2})_{Pt}$ as a reference, the enhancement factor for IR absorption of CO adsorbed on the nm-Ru/GC electrode is 19.8 by using Equation 2.

In the spectrum of a nm-PtRu/GC(4:6) alloy electrode, we again observe two positive-going CO_{ad} bands, CO_L and CO_B. The IR features of CO_{ad} bands on a PtRu alloy thin film may be regarded as a certain combination of IR features of CO_{ad} bands of nm-Pt/GC and those of nm-Ru/GC electrodes. The centre of the CO_L band is shifted negatively to 2048 cm^{-1}, and the FWHM of CO_L becomes larger and is measured at 43 cm^{-1}. It is obvious that the values of both the FWHM and CO_L band centre are between the values measured on the spectrum of nm-Pt/GC and those on the spectrum of nm-Ru/GC. Using $(A_{CO}/A_{CO_2})_{Pt}$ as a reference, the enhancement factor of IR absorption of CO adsorbed on a nm-PtRu/GC(4:6) electrode is calculated at 12.8.

The above results demonstrate clearly that electrodes of nanometer thin film materials manifest abnormal IR features for CO adsorption. These particular properties of nanometer thin film materials were termed abnormal infrared effects (AIREs) [24, 30], and consist mainly in three aspects: (i) inversion of the direction of the IR band, (ii) significant enhancement of IR absorption, and (iii) increase in FWHM of the IR band.

To clearly illustrate AIREs, single-beam spectra collected at $E_S = 0.0\,V$ ($R(E_S)$) and those at E_R ($R(E_R)$) on different electrodes are shown in Figure 4A. We observe from each $R(E_R)$ a negative-going band near 2345 cm^{-1} ascribed to IR absorption of solution CO_2 species. This band manifests a slightly larger intensity than that of the background; that is, IR absorption of gaseous CO_2

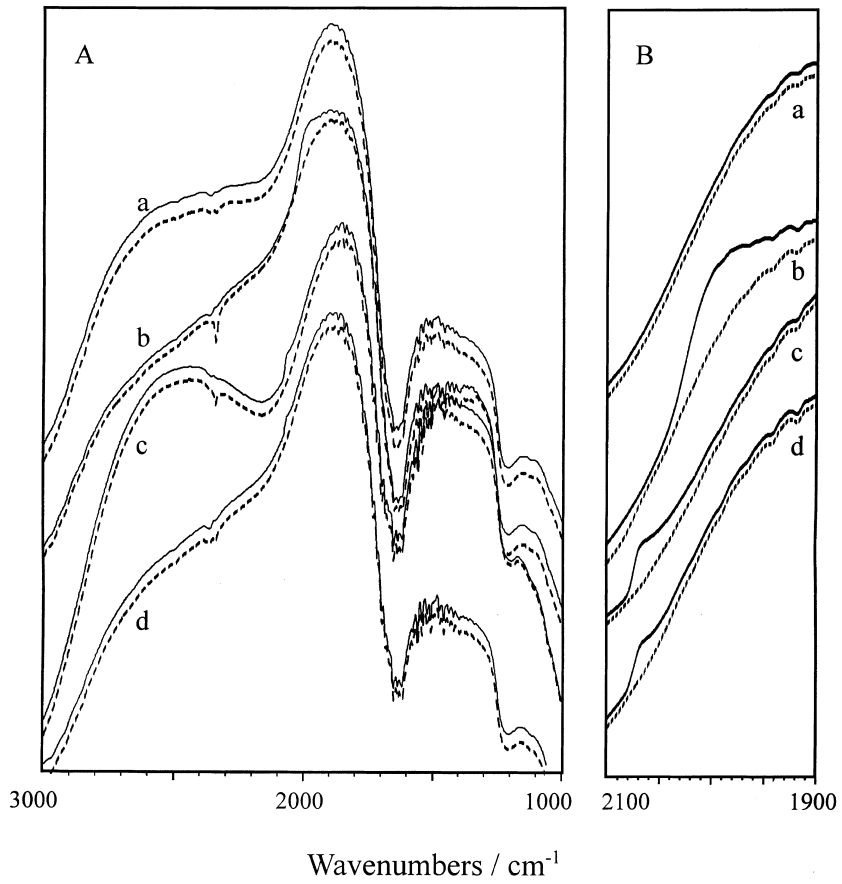

Fig. 4. Comparison of *in situ* single-beam spectra recorded at E_S (solid line) and E_R (dashed line) on Pt (a), nm-Ru/GC (b), nm-PtRu/GC (c) and nm-Pt/GC (d) electrodes. (A) 3000 ~ 1000 cm^{-1}, (B) 2100 ~ 1900 cm^{-1} with enlarged Y-scale.

species existing in the compartment of the optical bench of FTIR instrument that can be noticed from the corresponding $R(E_S)$. Although no IR band in the wavenumber region between 1900 and 2100 cm^{-1} was observed from the $R(E_S)$ of Pt electrode, a positive-going band appeared clearly in the $R(E_S)$ of the other three thin film electrodes. Figure 4B shows a comparison of $R(E_S)$ with $R(E_R)$ on an enlarged Y-scale. Figure 4 demonstrates clearly that CO adsorbed on nanometer thin film electrodes, that is, on nm-Pt/GC, nm-Ru/GC and nm-PtRu/GC, shows enhancement of IR absorption and inversion of the IR band direction.

A series of spectra for CO adsorbed on a nm-PtRu/GC(4:6) electrode recorded at different E_S is displayed in Figure 5(a). Three positive-going bands (i.e., the CO_2 band near 2343 cm^{-1}, the CO_L band around 2048 cm^{-1} and the small, but broad, CO_B band close to 1820 cm^{-1}) appear in all spectra. Following the increase in E_S from -0.25 to 0.05 V the CO_L band centre shifted positively to higher wavenumbers. The linear variation of the CO_L band centre against E_S is plotted in Figure 5(b); from the slope of the straight line the Stark turn rate was measured at 31 cm^{-1} V^{-1}. It is interesting to see that the CO_B band is also shifted positively to higher wavenumbers as E_S increases. However, determination of the CO_B band centre cannot be done precisely due to the wide spread of this band. As a consequence calculation of the Stark turn rate of this band could not be accomplished.

Three spectra between 2150 and 1750 cm^{-1} recorded on nm-PtRu/GC(4:2), nm-PtRu/GC(4:6) and nm-PtRu/GC(4:8) electrodes are compared in Figure 6. Following the increase in Ru in the PtRu alloy four features may be identified from these spectra. (i) A blue shift of the CO_L band is noticed. The band centre is measured near 2061 cm^{-1} on a nm-PtRu/GC(4:2) surface, but at around 2048 cm^{-1} on a nm-PtRu/GC(4:6); (ii) on the nm-PtRu/GC(4:8) electrode the CO_L band is shifted further to the lower wavenumber region, and it seems that the band is split into two peaks, one main peak near 2035 cm^{-1} and a shoulder peak close to 2024 cm^{-1}; (iii) the FWHM is increased from 24, 43 to 53 cm^{-1}; (iv) abnormal infrared effects can be observed on all nm-PtRu/GC electrodes, and the enhancement factor of IR absorption for CO adsorbed on these nm-PtRu/GC electrodes has been measured between 10.5 and 13.1. The above IR features are listed in Table 2 in comparison with data obtained on a massive Pt, a nm-Pt/GC and a nm-Ru/GC electrode. As discussed previously, the integrated intensity of the CO_2 band (A_{CO_2}) that represents the quantity of CO adsorbed in saturation on an electrode may be in direct proportion to the surface roughness of the electrode. In a similar way, the relative roughness may also calculated by using $A_{CO_2}/(A_{CO_2})_{nm\text{-}Pt/GC}$. From values listed in Table 2 we can see that all nm-PtRu/GC alloy electrodes and the nm-Ru/GC electrode have relatively higher surface roughness than the nm-Pt/GC electrode, which is similar to the conclusion drawn from data listed in Table 1. The fact that all nm-PtRu/GC alloy electrodes and the nm-Ru/GC electrode possess a smaller enhancement factor of IR absorption of CO_{ad} demonstrates that the calculation of Δ is independent of surface roughness. We have shown that the Δ may depend on the surface composition of the thin film electrode, and especially that the Δ varies considerably with the film thickness of

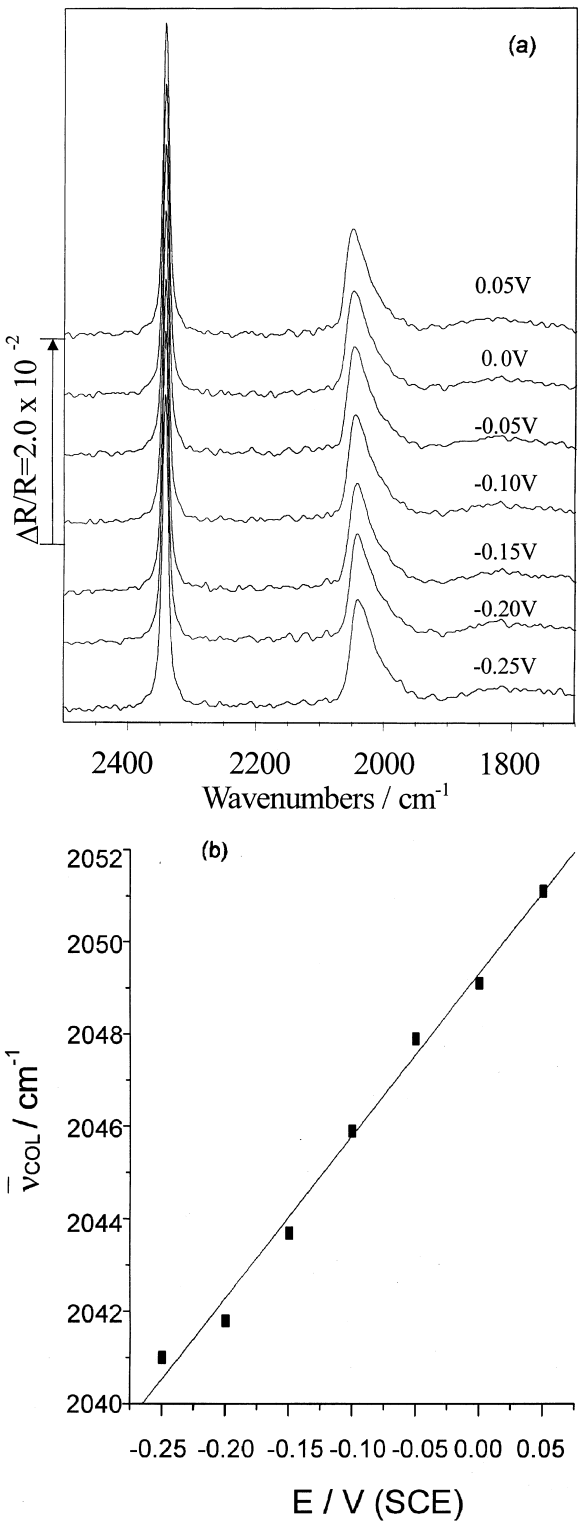

Fig. 5. (a) *In situ* FTIR spectra of CO adsorbed on nm-PtRu/GC(4:6) electrode at different E_S. 0.1 M $HClO_4$ solution, $E_R = 0.7$ V, E_S is indicated on each spectrum. (b) Plot of $\bar{\nu}_{COL}$ against E_S.

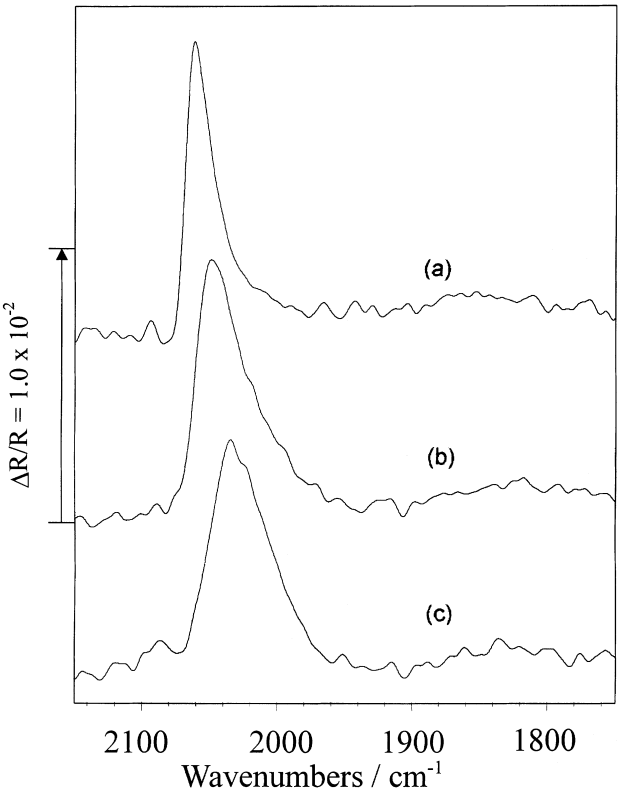

Fig. 6. Comparison of spectra of CO adsorbed on (a) nm-PtRu/GC(4:2), (b) nm-PtRu/GC(4:6) and (c) nm-PtRu/GC(4:8) electrodes. 0.1 M $HClO_4$ solution, E_S = 0.0 V, E_R = 0.7 V.

transition metal or alloy electrodeposited on glassy carbon [36,37].

3.3. *Scanning tunnelling microscope (STM)*

The nm-PtRu/GC alloy electrode exhibited a high activity for CO_{ad} oxidation and abnormal infrared effects; these properties may relate to the particular structure of PtRu alloy thin film. The STM images of a nm-PtRu/GC(4:1) and a nm-PtRu/GC(4:8) are shown in Figure 7. In order to see the evolution of crystallite structure the STM image of a nm-Pt/GC electrode is also displayed in the same figure. The nm-Pt film is composed of crystallites in a cubic form, clearly showing a face centred cubic (f.c.c.) structure. The width and the length of each crystallite are respectively around 200 and 250 nm, nevertheless the thickness (or the height) ranges only between 20 and 25 nm. Significant changes were observed in the image of the nm-PtRu/GC(4:1) electrode. The crystallites of PtRu(4:1) alloy appear to be hexagonal in form. The dimension of each crystallite is around 300 nm with a thickness of about 10 nm only. When the component of Ru is increased in the nm-PtRu thin film, that is, for an electrode of nm-PtRu/GC(4:8), the crystallites are still in a hexagonal-like form of dimension around 300 nm and thickness about 15 nm. It is interesting to observe some fine structures on the crystallites, that is, one or two scratches appeared on the top of each crystallite of nm-PtRu(4:8) alloy. This may imply that some kind of twin crystallite of PtRu alloy may be formed. Richard et al. [21] reported that the surface composition of PtRu alloy prepared by electrochemical codeposition depends on the percentage Pt in the solution, and a linear relationship was obtained when the percentage Pt in solution was above 20%. They found by X-ray photoelectron spectroscopy (XPS) and low energy ion spectroscopy (LEIS) analysis that the molar fraction of Pt in the surface is always higher than that of the deposition solution. The above STM results indicate that the crystallites of electrodeposited PtRu alloy tend to grow in hexagonal form of layered structure, even with a composition of 4:1 (Pt:Ru) at which the f.c.c. structure was determined for bulk PtRu alloy with X-ray diffraction [38].

It may be worth pointing out that the crystallites of layered structure were observed in all STM images of different nanometer thin film electrodes [30, 39]. This layered structure is different from that of thin film electrodes prepared under normal deposition conditions (at constant current or potential), which often growth in island structure. The layered structure of nanometer thin film may be attributed to one of the reasons for the AIREs [30].

4. Conclusions

In the present work, emphasis has been laid on the structure and properties of nanometer thin films of PtRu alloy. Electrochemical codeposited PtRu alloy thin films under cyclic voltammetric conditions and supported on glassy carbon substrate (nm-PtRu/GC) show particular structures. STM images show that the crystallites of PtRu alloy film have a hexagonal layered structure, even with a small quantity of Ru component in the alloy. The crystallites of PtRu alloy are about 300 nm in size with a

Table 2. IR parameters acquired on different electrodes

Electrode	ν_{COL} /cm^{-1}	FWHM of ν_{COL}/cm^{-1}	$A_{CO_{ad}}$	A_{CO_2}	$A_{CO_{ad}}/A_{CO_2}$	Δ	$A_{CO_2}/(A_{CO_2})_{nm\text{-}Pt/GC}$
Pt	2082	14	1.72	13.13	0.13	–	0.56
nm-Pt/GC	2074	20	86.29	23.82	3.62	27.8	1.00
nm-PtRu/GC(4:2)	2061	24	48.14	35.15	1.36	10.5	1.48
nm-PtRu/GC(4:6)	2048	43	64.60	38.72	1.67	12.8	1.60
nm-PtRu/GC(4:8)	2035, 2024	53	56.65	33.39	1.70	13.1	1.40
nm-Ru/GC	2017	55	110.42	42.84	2.58	19.8	1.80

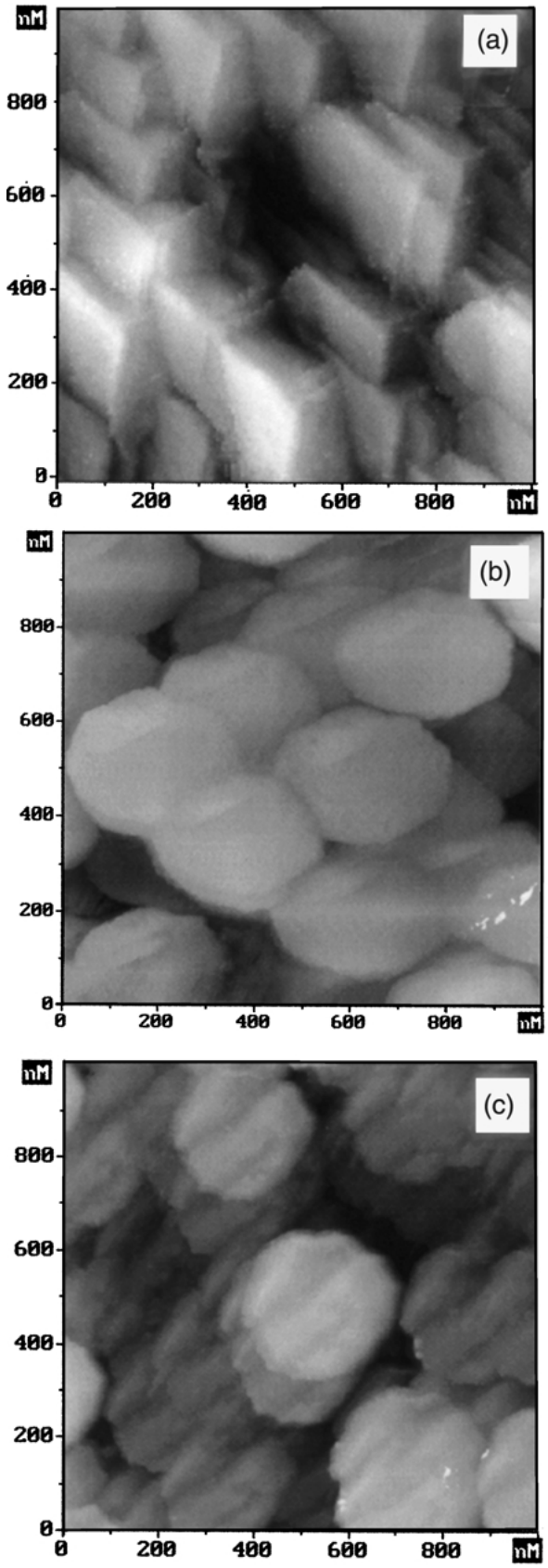

Fig. 7. STM images. (a) nm-Pt/GC, I_t = 0.274 nA, V_b = 0.130 V; (b) nm-PtRu/GC(4:1), I_t = 0.504 nA, V_b = 0.060 V; (c) nm-PtRu/GC(4:8), I_t = 0.093 nA, V_b = 0.170 V.

thickness ranging between 10 and 15 nm. Cyclic voltammetric studies showed that the PtRu alloy thin film materials possess high activity towards the oxidation of adsorbed CO. The potential of oxidation of CO_{ad} on nm-PtRu/GC was decreased by more than 200 mV in comparison with that of CO_{ad} oxidation on nm-Pt/GC, and the normalized rate of CO_{ad} oxidation is much faster on nm-PtRu/GC than that on nm-Ru/GC. The *in situ* FTIR spectroscopic investigations demonstrated that the nanometer thin film of PtRu alloy, similar to the nanometer thin film material of transition metals, exhibited abnormal infrared effects (AIREs) for CO adsorption. Three main characters of AIREs have been confirmed with nm-PtRu/GC electrodes, that is, inversion of the direction of CO_{ad} bands, significant enhancement of IR absorption of CO_{ad}, and enlargement of the FWHM of CO_{ad} bands. The enhancement factor of IR absorption of CO_{ad} on nm-PtRu/GC electrodes has been evaluated between 10.5 and 13.1, which is smaller than that measured on both nm-Pt/GC (27.8) and nm-Ru/GC (19.8) electrodes. The results obtained in the present study have thrown light on the structure and properties of nanometer thin film materials of PtRu alloy, especially on the electrocatalytic effects towards CO_{ad} oxidation and the abnormal infrared effects that relate to the nanometer size effects. The study highlights the possible use of nanometer scale thin film PtRu alloy material in fuel cell applications.

Acknowledgement

This work was supported financially by Natural Science Foundation of China (NSFC).

References

1. S. Gttesfeld, Polymer electrolyte fuel cells, *in* R.C. Alkire, H. Gerischer, D.M. Kolb and C.W. Tobias (Eds), 'Advances in Electrochemical Science and Engineering', Vol. 5 (Wiley–VCH, Inc., 1997).
2. H. Wendt and C. Lamy (Eds), Abstracts volume of workshop for 'Electrocatalysis in Indirect and Direct Methanol Fuel Cells', Portorose, Slovenia, 12–14 Sept. (1999).
3. C. Lamy, J.-M. Léger and S. Srinivason, Direct methanol fuel cells from a 20th century electrochemists dream to a 21th century engineering technology, *in* J.O'M. Bockris (Ed.), 'Modern Aspects of Electrochemistry', Vol. 34 (Plenum, New York, 1999).
4. C.E. Lee and S.H. Bergens, *J. Phys. Chem. B* **102** (1998) 193.
5. M. Watanabe, Y. Genjima and K. Turumi, *Denki Kagaku* **64** (1996) 462.
6. J.C. Davies, B.E. Hayden and D.J. Degg, *Electrochim. Acta* **44** (1998) 1181.
7. W. Charzanowski and A. Wieckowski, *Langmuir* **14** (1998) 1967.
8. W. Chrzanowski, H. Kim and A. Wieckowski, *Catal. Lett.* **50** (1998) 69.
9. K.A. Friedrich, K-P. Geyzers, U. Linke, U. Stimming and J. Stumper, *J. Electroanal. Chem.* **402** (1996) 123.

10. T.J. Schmidt, M. Noeske, H.A. Gasteiger, R.J. Behn, P. Britz and H. Bonnemann, *J. Electrochem. Soc.* **145** (1998) 825.
11. T.J. Schmidt, M. Noeske, H.A. Gasteiger, R.J. Behm, P. Britz, W. Brijoux and H. Honnemann, *Langmuir* **13** (1997) 2591.
12. D.R. Rolison, P.L. Hagans, K.E. Swider and J.W. Long, *Langmuir* **15** (1999) 774.
13. N.M. Markovic, H.A. Gasteiger, P.N. Ross, X.D. Jiang, I. Villegas and M.J. Weaver, *Electrochim. Acta* **40** (1995) 91.
14. P.N. Ross, *Electrochim. Acta* **36** (1991) 2053.
15. A. Kabbabi, R. Faure, R. Durand, B. Beden, F. Hahn, J.M. Leger and C. Lamy, *J. Electroanal. Chem.* **444** (1998) 41.
16. W.F. Lin, T. Iwasita and W. Vielstich, *J. Phys. Chem. B.* **103** (1999) 3250.
17. T. Iwasita, F.C. Nart and W. Vielstich, *Ber. Bunsenges. Phys. Chem.* **94** (1990) 1030.
18. K. Wang, H.A. Gasteiger, N.M. Markovic and P.N. Ross, Jr., *Electrohim. Acta* **41** (1996) 2587.
19. R. Ianniello, V.M. Schmidt, U. Stimming, J. Stumper and A. Wallau, *Electrochim. Acta* **39** (1994) 1863.
20. H.A. Gasteiger, N. Markovic, P.N. Ross, Jr. And E.J. Cains, *J. Phys. Chem.* **98** (1994) 617.
21. F. Richarz, B. Wohlmann, U. Vogel, H. Hoffschulz and K. Wamdelt, *Surf. Sci.* **335** (1995) 361.
22. E. Jusys, H. Massong and H. Baltruschat, *J. Electrochem. Soc.* **146** (1999) 1093.
23. A. Kelaidopoulou, E. Abelidou, A. Papiutsis and E.K. Polychroniadis, *J. Appl. Electrochem.* **28** (1998) 1101.
24. G-Q. Lu, L-R. Cai, S-G. Sun and J-X. He, *Chinese Science Bulletin* **42** (1999).
25. M. Watanabe, M. Uchida and S. Motoo, *J. Electroanal. Chem.* **229** (1987) 395.
26. S-G. Sun, Studying electrocatalytic oxidation of small organic moleculars with *in situ* infrared spectroscopy, *in* J. Lipkowski and P.N. Ross (Eds), 'Electrocatalysis' (Wiley-VCH, 1998), chapter 6, pp. 243–290.
27. W-F. Lin and S-G. Sun, *Electrochim. Acta* **41** (1996) 803.
28. G-Q. Lu, S-G. Sun, S-P. Chen and L-R. Cai, *J. Electroanal. Chem.* **421** (1997) 19.
29. G-Q. Lu, S-G. Sun, S-P. Chen, L-R. Cai and Z-W. Tian, *Chem., J. Chinese Univ.* **18** (1997) 1491.
30. G-Q. Lu, S-G. Sun, L-R. Cai, S-P. Chen, Z-W. Tian and K-K. Shiu, *Langmuir* **16** (2000) 778.
31. A.E. Bjerke, P. Griffiths and W. Thesis, *Anal. Chem.* **71** (1999) 1967.
32. R. Oritz, A. Cuesta, O.P. Marquez, J. Marquez, J.A. Mendes and C.J. Gutierrez, *J. Electroanal. Chem.* **465** (1999) 234.
33. N.P. Lebedeva, G.N. Kryukova, S.V. Tsybulya, A.N. Salanov and E.R. Savinova, *Electrochim. Acta* **44** (1998) 1431.
34. R.C. Walker, M. Bailes and L.M. Peter, *Electrochim. Acta* **44** (1998) 1289.
35. E. Ticanelli, J.G. Beery, M.T. Paffett and S. Gottesfeld, *J. Electroanal. Chem.* **258** (1989) 61.
36. G-Q. Lu, S-G Sun, S-P. Chen, N-H. Li, Y-Y. Yang and Z-W. Tian, *in* A. Wieckowski and K. Itaya (Eds), 'Electrode Processes' (Electrochemical Society, Pennington, NJ, 1996), PV 96–8.
37. M-S. Zheng and S-G. Sun, *J. Electroanal. Chem.* submitted.
38. H.A. Gasteiger, P.N. Ross, Jr and E.J. Cairns, *Surf. Sci.* **293** (1993) 67.
39. G-Q. Lu, PhD thesis, Xiamen University (1997).